Formation Imaging from Three-Component Borehole-Seismic Data Using both Space-time Relations and Wave-Field Polarization

Jakob B.U. Haldorsen, Tor Hilton, Mathieu Milenkovic, READ AS; Marco C. Schinelli, Lucas Furtado Soares, Jose E. M. Lira, and Ana Zelia Nunes de Barrio, Petrobras

Copyright 2013, SBGf - Sociedade Brasileira de Geofísica

This paper was prepared for presentation during the 13th International Congress of the Brazilian Geophysical Society held in Rio de Janeiro, Brazil, August 26-29, 2013.

Contents of this paper were reviewed by the Technical Committee of the 13th International Congress of the Brazilian Geophysical Society and do not necessarily represent any position of the SBGf, its officers or members. Electronic reproduction or storage of any part of this paper for commercial purposes without the written consent of the Brazilian Geophysical Society is prohibited.

Abstract

An array of multi-component receivers used to acquire borehole-seismic data allows for measuring the compressional and shear components of a wave field from within the rock volume itself. Having determined the polarizations and the arrival times of the different components over the aperture of the array, we estimate their direction of propagation. The propagation direction essentially points back to the point of reflection, scattering or conversion.

We describe how a ray-based migration/deconvolution process could be used to separate the scattered compressional component from other wave-field components by projecting the full 3C wave field on to or perpendicular to the ray connecting the receiver and image point. These components were used to give images from a 2D spread of source locations.

Introduction

Borehole-seismic data, more commonly called Vertical Seismic Profiling (VSP), are widely used to generate maps of vertical seismic travel times versus formation depth. Such maps are important in order to estimate vertical formation velocities, otherwise not well constrained by surface-seismic data. However, used for imaging, VSP data have a credibility issue related to an apparent inability to deliver on a long-held promise of providing images at higher resolution than what normally can be obtained from corresponding surface-seismic data. The reason why one should expect higher resolution from VSP data compared to surface-seismic data is that, with the acoustic receivers in the formation, the acoustic waves have traversed less rock on their way from the source to the receivers, preserving more of the high frequencies in the data.

The acoustic waves used in the VSP survey are generated by an acoustic source on the surface and recorded by three-component (3C) receivers in the well. The 3C receivers measure three orthogonal components of particle movement generated by a wave front passing the receiver.

The multi-level aspect of the receiver array will allow the estimation of delay from one receiver to the next while the wave front is passing from one end of the array to the other. The multi-level 3C receiver array can therefore be used to find estimates of both the full waveform and the direction of propagation in 3D space of any passing plane waves, arriving either directly from the source or scattered by the formation. If the formation velocities are known at some level of accuracy, the time delays and polarizations at the array of receivers are sufficient for identifying whether the passing wave was compressional or shear (Leaney and Esmersoy, 1989), the ray direction, and the distance along the ray back to the source, or the location where the compressional and shear waves coincide in time and space (e.g., Haldorsen et al., 2009, 2012).

The two basic processes for generating images from seismic reflection data are deconvolution and migration: Simply put, deconvolution compresses the signal of the seismic source to a spike, and migration transforms the map of reflection times to a volumetric map of formation properties. Conventionally, the deconvolution is applied first, followed by the migration. However, analyzing the imaging process as an inverse scattering problem, one is led to conclude that the deconvolution should fundamentally be seen as part of the migration process.

For each point in image space, combining the wave field polarization measured by the 3C receiver, with the space-time relationship offered by the wave equation, one may be able to generate complete estimates of both the source field and the scattered fields over a reasonably large section of space surrounding the data acquisition site.

Deconvolving the “scattered” wave field by the “source” wave field is the conditioning that converts the map of scattering times to a map of changes in acoustic impedance.

Elements of the Scattering Matrix

The Scattering Matrix **S**, is the ratio of the properly normalized displacement vectors for the scattered and the incoming fields (Aki and Richard, 2009, Chapter 5). Simply put, **S**(**x**) consists of measures of the relative changes in acoustic properties of the medium at location **x**. If both the source and scattered wave fields are measured in the same units, after a deconvolving the last by the first, one is left with direct measurements of elements of **S**(**x**). These direct estimates can strictly only be made for the formation at or near the receiver stations. Extrapolating from the sources and receivers to each point in image space, one will have to find estimates for both the incoming and scattered wave fields – extrapolating from the receivers over a shorter distance with a VSP geometry than with a surface-seismic geometry.

For a given angular frequency ω, wave-number vector $\mathbf{k}_i$ for incoming wave, and $\mathbf{k}_o$ for outgoing wave (with $|\mathbf{k}|=\omega/c$), taking the ratio of these two extrapolated wave fields gives a measure of $\mathbf{S}(\mathbf{k}_o - \mathbf{k}_i)$ at one single wave-number vector $\mathbf{k}_o - \mathbf{k}_i$. To make estimates over a larger section of the 3D $\mathbf{k}$ space, one would need to increase the spatial range as well as the frequency range over which the data are acquired. The large scattering angle associated with forward scattering results in a low value to $|\mathbf{k}| = |\mathbf{k}_o - \mathbf{k}_i|$ because of the small angle between the vectors $\mathbf{k}_o$ and $\mathbf{k}_i$. A practical discussion of these issues can be found in Haldorsen and Farmer (1989). Most commonly, these low-frequency effects are referred to as "NMO stretch" and the "artifacts" reduced by applying far-offset mute to the data, thereby removing potentially valuable information about the low-frequency formation trends.

Deconvolution and Migration

Elements of the Scattering Matrix $\mathbf{S}(\mathbf{x})$ at an image point $\mathbf{x}$ can be found by deconvolving the extrapolated scattered field at $\mathbf{x}$ by the corresponding source wave field $\mathbf{D}(\tau_{\mathbf{sx}},\mathbf{p}_{\mathbf{sx}})$. If the two are coincident in time at $\mathbf{x}$, the maximum amplitude for the deconvolved waveforms will be at zero, local time. In this way, the wave-field deconvolution is part of the imaging condition for the migration process.

As the estimated incoming, source wave field would be spatially variant, in all but very special circumstances, the wave-field deconvolution and the wave-field migration do not commute and the deconvolution should be done inside the kernel of the migration process at each individual point within image.

Much effort has gone into finding simplifications that would allow separating the deconvolution and the migration processes. Possibly one of the most common and far-reaching simplifications is derived from the assumption of a point source in a homogeneous formation. This would give a source field that is spatially invariant, allowing the deconvolution to be factored out and applied to the raw data prior to migration. As a consequence, the imaging condition applied in the migration is travel-times only. However, even in the simplest case of marine data, the presence of the air-water interface near the source gives a source signature that is highly dependent on the radiation angle. Other formation features would similarly affect the signature of the source wave field.

Reverse-time migration

The projection from the borehole into the 3D formation can be done using the Reverse-time Migration (RTM) described by, e.g., Chang and McMechan (1986), or Schuster (2002). In the RTM process, the wave equation is run in reverse, injecting the recorded wave field back into a model with known velocities, calculating the full wave field that could possibly have been generated at any point in the 3D volume. Each shot is modeled forward in time from the location from the shot to each of the image points, where the scattering strength is found as the correlation coefficient (zero-lag correlation) of the two extrapolated wave fields. As argued above, wave-field correlation should be replaced by wave-field deconvolution. Correlation is kinematically equivalent to deconvolution, but, although more stable, is dynamically different. With non-white, extrapolated source wave-fields, the use of correlation instead of deconvolution would give an image with lower bandwidth and resolution. Depending on the accuracy of the velocity model used to extrapolate the source wave field, the instabilities introduced by a deconvolution process may be significant. These instabilities could possibly be controlled by using a Wiener-style deconvolution operator, similar to the operator described by Haldorsen et al. (1994).

The RTM process can in principle be iterated with a gradually refined model and more accurate wave equation. Carefully done, this process would give the correct image, using all available information about the propagating wave fields.

RTM is, even when it is not iterated, quite computer and memory intensive. However, depending on the complexity of the velocity model used, and the completeness of the wave equation, the image obtained from an RTM scheme would include contributions from components of the wave field that have been scattered more than once.

Ray-based Migration (Wave Field Extrapolation)

A faster, but less general migration scheme is based on the plane-wave decomposition, each plane-wave component corresponding to a single value of the ray-vector $\mathbf{k}$. Using the ray concept, one may analyze and better understand certain aspects of the migration and deconvolution process. In the following, we will stay in this $\mathbf{k}$-domain.

For a given source-receiver pair, the waves scattered off or converted at a formation structure will have distinct propagation directions and polarizations. A given particle motion as measured by the VSP tool at the borehole wall, could be caused by either a compressional wave or a shear wave. In assuming that the compressional field is polarized along the ray connecting the scattering/conversion point to the receiver location, and that the polarization of the shear is perpendicular to this ray, Haldorsen (2002) shows that vector-based migration using travel times in combination with polarization is sufficient for separating compressional and shear contributions into two separate images, and allowing the wave-field separation to be done inside the migration kernel by projecting the recorded wave fields onto and perpendicular to the connecting rays.

For simple velocity structures, the time delays and ray parameters can be estimated from ray tracing, and the components of an elastic wave field can be found by process of Haldorsen (2002). For a definite time window n, the P time-series signature $f^{P}_{nk}(\omega)$ for voxel k is found from focusing the projections of the recorded 3C data $\mathbf{d}_{jn}(\omega)$ for receiver level j, onto the ray vector $\mathbf{p}_{jk}$ at the receiver (ω denotes the angular frequency).

The ray vector $\mathbf{p}_{jk}$ can be found by tracing rays through a velocity model from voxel k to receiver j. Similarly, the S time-series signatures are found from focusing the projections perpendicular to the ray vector. The focusing is achieved by stacking after the delaying the projections of the recorded field by the appropriate travel times, $t^{P,S}_{jK}$:

$$f^{P}_{nk}(\omega) = \frac{1}{N_r}\sum_{j=1}^{N_r} \mathbf{p}^{P}_{jk} \bullet \mathbf{d}_{jn}(\omega)\, A^{P}_{jk} e^{-i\omega t^{P}_{jk}} \quad (1)$$

$$f^{Sv}_{nk}(\omega) = \frac{1}{N_r}\sum_{j=1}^{N_r} [\mathbf{p}^{Sv}_{jk} \times \mathbf{d}_{jn}(\omega)]_T\, A^{Sv}_{jk} e^{-i\omega t^{Sv}_{jk}} \quad (2)$$

$$f^{Sh}_{nk}(\omega) = \frac{1}{N_r}\sum_{j=1}^{N_r} [\mathbf{p}^{Sh}_{jk} \times \mathbf{d}_{jn}(\omega)]_V\, A^{Sh}_{jk} e^{-i\omega t^{Sh}_{jk}} \quad (3)$$

where, A_{jk} is the inverse of the geometric-spreading term extrapolating from the location of voxel k to receiver j. The subscript "T" denotes the horizontal component of the vector product, and "V" the component perpendicular to the "T" component. Whereas equation (1) measures the divergent ("curl-free", or compressional) part of the wave field, equations (2) and (3) measure the "divergence-free" (or shear) part of the wave field. In a homogeneous, isotropic formation, the operations described by equations (1), (2), and (3), correspond to integrating around a sphere centered on the source, the component of the wave field perpendicular to the sphere (equation (1) for estimating the signature of the scattered P signal) and the two components tangential to the sphere (equations (2) and (3) for estimating the signatures of the scattered S signal). These estimates of the scattered signals should subsequently be deconvolved by the estimates of the source signal, described below.

The wave-field decomposition achieved by applying the vector migration concepts are similar to the parametric decomposition described by Leaney and Esmersoy, 1989.

In Haldorsen et al. (2009, 2013) this concept was extended using direct compressional and converted shear in order to image structures above and to the side of the VSP tool; and by Cheng et al. (2010) for whole-earth seismics to image the MOHO about 40 km below an array in Northern Canada. The projection technique used in either of these two papers can straightforwardly be extended to 3D, allowing the generation of partial images in 3D space from an individual offset VSP acquired with 3C receivers. This process is guided by the polarization and propagation direction of the recorded wave field and the travel times derived from a velocity model, either pre-existing or otherwise derived from the data.

Deconvolution of 3D VSP data

Acquiring a 3D VSP, one generally would use sources, distributed in some 2D pattern across the surface. With a 2D source spread, the VSP receiver array allows for the estimation of the down-going field $\mathbf{D}(\tau,\mathbf{p_{sr}})$ as a function of the source-receiver ray parameter $\mathbf{p_{sr}}$ and arrival time $\tau_{\mathbf{sr}}$.

We make the simplifying assumption that the down-going field depends only on $(\tau,\mathbf{p})$ - and thus is invariant under transverse, horizontal translation. This does allow for limited azimuthal anisotropy, showing in the dependence of $\mathbf{D}(\tau,\mathbf{p})$ on the horizontal components of the ray parameter $\mathbf{p}$. If the formation does not exhibit measurable azimuthal anisotropy, this would simplify the process by allowing $\mathbf{D}(\tau,\mathbf{p})$ to be both translational and rotational invariant (meaning that the medium is "1D", VTI). This assumption of symmetry is similar to the one used by Brandsberg-Dahl et al. (2007). They extract the Green's functions $G(\mathbf{x}_s,\mathbf{x}_r,\omega)$ for the overburden from walk-away VSP data. Here $\mathbf{x}_s$ and $\mathbf{x}_r$, are the locations of a source and a receiver. The assumption of translational invariance allows them to derive an inverse of the Green's function that may be applied to the surface-seismic data, acquired concurrent or not with the walk-away VSP data. Within the image-cube for a 3D VSP dataset, the areal extent of the assumed translational invariance would be significantly smaller for our application than for an operator to be applied to a surface-seismic dataset.

Elements of the Scattering Matrix $\mathbf{S}(\mathbf{x})$ at each sub-surface image point $\mathbf{x}$ is found by deconvolving the extrapolated scattered field at $\mathbf{x}$ by the corresponding source wave field $\mathbf{D}(\tau_{\mathbf{sx}},\mathbf{p_{sx}})$. The deconvolution can be made to be of the Wiener type by, e.g., including semblance weights. This would be a straightforward extension of the method described by Haldorsen et al. (1994), or Haldorsen et al. (2004). Their operator is designed to broaden the spectrum of the estimated source signal at the same time as minimizing any additional signal present in the data. Using ω for the angular frequency, in the $(\omega,\mathbf{p_{sx}})$ frame of reference, the extended operator may possible look like:

$$F_n(\omega,\mathbf{p_{sx}}) = \frac{f^{*}_n(\omega,\mathbf{p_{sx}})}{E_n(\omega,\mathbf{p_{sx}})} = \frac{f^{*}_n(\omega,\mathbf{p_{sx}})}{|f^{*}_n(\omega,\mathbf{p_{sx}})|^2}\,\frac{|f^{*}_n(\omega,\mathbf{p_{sx}})|^2}{E_n(\omega,\mathbf{p_{sx}})} \quad (4)$$

where $E_n(\omega,\mathbf{p_{sx}})$ is the frequency-domain estimate of the total energy at depth level n in the direction in the direction $\mathbf{p_{sx}}$, and $f_n(\omega,\mathbf{p_{sx}})$ is the source signal at the same depth level, estimated from the 3C data vector $\mathbf{e}_j$ at level j:

$$f_n(\omega,\mathbf{p_{sr}}) = \frac{1}{2k+1}\sum_{j=n-k}^{n+k} \mathbf{p_{sr}} \bullet \mathbf{e}_j(\omega)\, e^{-i\omega\tau_{sr}} \quad (5)$$

The compressional source function measured by equation (5) is the raw function generated at the physical source, after having been modified by propagation from the source to the receiver array. This modified source function will contain components scattered from inhomogeneities underway. However complicated the primary compressional signal is, the secondary scattered and converted components of the wave field will have the same inherent complexity. The filter given by equation (4) will compress both the compressional source wave field and any other wave field that is coherent with this, including the converted down-going shear components of the wave field. Within its range of validity, deconvolving the total recorded using equations (5) and (4) is therefore expected to be well suited for imaging using ray-based migration.

A point refractor will generate wave fields with distinct radiation pattern for both compressional and converted shear. With a wide enough acquisition aperture, it is

commonly assumed that the migration operation will sort out these radiation patterns as images are formed by stationary-phase sums along coherent wave fronts.

For a complete description of the medium, in addition to the compressional components, one would need to consider two sets of shear components for both the incoming and the scattered or transmitted wave fields.

Energy-flux density, illumination

Combining multiple measurements, either overlapping in **k**-space or not, one has to account for variation of the energy-flux density related to formation and acquisition geometries for both the incoming and the reflected wave fields.

The concept of "fold" used in the seismic industry is a simple measure of illumination. In acquisition of surface-seismic data, the fold is normally defined as the number of source-receiver midpoints within a certain patch on the surface equal in size to an image pixel. An "even fold" is generally taken to mean an even 2D distribution on the surface of midpoints between sources and receivers. However, if the formation is not translational invariant (Vertical Transverse Isotropic, or VTI) an even distribution of sources on the surface may easily result in an un-even distribution of illumination, or flux density, in the subsurface. What one should really want to achieve is an even distribution in "image space" for the spatial wave numbers, k, for the image, or even distribution for the wave-field "kick" $\mathbf{k}_o$ - $\mathbf{k}_i$. Using appropriate weighting, this can be obtained using a source with a wide spectral bandwidth, and an even angular distribution. An even distribution of sources on the surface, gives a larger flux density at shallow image depth for large angles to the vertical than for small angles to the vertical, leading to an overrepresentation of low frequencies in an image obtained by Kirchhoff migration. Miller, Oristaglio, and Beylkin (1987) give the prescriptions on how to calculate the proper flux density as a function of angles. Their Jacobian term describes the weights necessary to get from, e.g., an even distribution on the surface to an even distribution of flux density around an image point. Applying their weights to the sums used in Kirchhoff migration, effectively weighs down, e.g., the low-frequency contributions to the seismic image originating from large-angle scattering common in seismic records at early times and large offsets.

To find correct estimates of the flux densities of the source and the scattered fields, one has to allow for focusing and defocusing of these fields along their paths of propagation through various types of acoustic lenses - as well as for their otherwise loss of energy due to, e.g., scattering and absorption.

Application

For a "zero-offset" VSP all down-going source energy, either primary or scattered or converted by a VTI formation, will propagate along the receiver array at the same ray direction $\mathbf{p}_{sx}$. Although any part of this energy modified by non-VTI components of the formation, will travel at a different ray angle, this is the assumption made by most standard processing of VSP data, allowing the migration and deconvolution operators to commute and the deconvolution operator to be applied pre-imaging.

Similarly, for a homogeneous, isotropic medium and a point source (isotropic radiation pattern), the incoming source signature is independent on $\mathbf{p}_{sx}$, and the source-deconvolution operator described by equation (2) will be independent on angles of incidence and commute with the migration operator.

For a straightforward test of the vector migration process, we assume that either of these conditions applies, allowing the two operators to commute. We determine the deconvolution operator from the down-going wave field and apply the semblance-weighted inverse of this to all traces prior to migration, allowing.

For the test, we use data acquired for Petrobras in a near-vertical well offshore Brazil. The two, near 2 km long, walk-away source lines run at 38 m intervals from South to North and from West to East, respectively. The two lines intersect very close to a platform. The geometry is illustrated in Figure 1. The 40 3C receivers were deployed in a near vertical well at 15.2 m interval from 5177 m to 5772 m. Figure 2 shows the raw, 3-component data recorded by the shallowest receiver along the two complete lines.

Figure 3 shows for both lines, for a source point near the platform: the raw data, the deconvolved data, and residuals after separating the down-going P from the deconvolved data. At the short horizontal offset between source and receivers, for both lines, the inline and transverse components of the residual deconvolved data show mostly down-going S, and the vertical components show mostly reflected P. The most prominent events include one close to 30% down the receiver array from the top, one just below the deepest receiver and one somewhat deeper.

In Figure 4, we show the P-reflection images obtained by vector migration of the residual deconvolved data, showing the three reflectors indicated by the data in Figure 3. These can be compared in Figure 5, to images obtained from surface-seismic data and the images obtained by conventional processing of the walk-away lines. Also shown for comparison to these and to the images in Figure 4, are the images obtained from vector migration, where we have compensated for varying fold (or energy flux density) as calculated for each pixel in the image.

For what we have labeled "conventional processing", the 3C data were converted to scalar data, before using the scalar wave equation for conventional migration imaging.

The most important differences between the conventional VSP image and the image obtained by vector migration are seen in the reflectors at the depths of around 6000 and 6500 m, hardly visible in the conventional processing. The West-to-East oriented image indicates a fault in the reflector at 6500 m just East of the well. This fault can also be inferred from the West-to-East surface-seismic image.

The shallowest of the three prominent reflectors already mentioned appears to be faded in the images in Figure 4. This is due to the fact that the energy reflected from this will only be seen by the few shallower receivers. Compensating for the decrease in image fold corrects for this dimming.

Conclusions

Using an array of multi-component receivers to acquire borehole-seismic data allowed us to measure the compressional and shear components of a wave field from within the rock volume itself. Having determined the polarizations and the arrival times of the different components over the aperture of the array, we estimate their direction of propagation. This propagation direction essentially points back to the point of reflection, scattering or conversion.

After some simplifying assumption, we have demonstrated the effectiveness over more conventional processing of using the full, 3-component data in a vector-migration process.

Acknowledgments

We thank the management of READ and Petrobras for supporting the development of the new imaging tools, and Petrobras for allowing this to be published.

References

Aki and Richard, 2009, Quantitative Seismology, 2nd edition chapter 5, University Science Books.

Brandsberg-Dahl, S., Xiao, X., and Hornby, B., 2007, Surface Seismic Imaging with VSP Green's Functions, paper H012, 69th Mtg.: Eur. Assn. Geosci. Eng., London, 2007.

Brooks, N.J., J.B.U. Haldorsen, M. Milenkovic, C. Crowell, and M.B. Farmani. A New Full-waveform, Migration-based Deconvolution Method Applied to Locating Microseismic Events in Canada. Paper C047, Extended Abstracts, 74th Mtg.: Eur. Assn. Geosci. Eng., Copenhagen, 2012.

Chang, W. F., and McMechan, G. A., 1986, Reverse-time migration of offset vertical seismic profiling data using the excitation-time imaging condition: Geophysics, **51**, 67-84.

Chen, C.-W., D.E. Miller, H.A. Djikpesse, J.B.U. Haldorsen, and S. Rondenay, 2010, Array-conditioned deconvolution of multiple component teleseismic recording, Geophys. J. Int., **182**, 967-976

Haldorsen, J. B. U. 2002, Converted-shear and compressional images using Projection Imaging. 64th EAGE Conference & Exhibition, Extended Abstracts, F031.

Haldorsen, J. B. U., Borland, W., and Heijna, H. B., 2004, Extended High-Frequency Processing Of Vibrator VSP Data, Extended Abstracts, 66th Mtg.: Eur. Assn. Geosci. Eng., Paris, 2004

Haldorsen, J. and Farmer, P. A., 1989, Resolution and NMO-stretch: imaging by stacking: Geophysical Prospecting, **37**, 479-492.

Haldorsen, J. B. U., W. S. Leaney, R. T. Coates, S. A. Petersen, H. I. Rutledal, and K. A. Festervoll, 2013, Imaging above an extended-reach horizontal well using converted shear waves and a rig source: Geophysics, **78**, 2, 1–11.

Haldorsen, J. B. U., W. S. Leaney, R. T. Coates, S. A. Petersen, H. I. Rutledal, and K. A. Festervoll, S. Hess, 2009, Converted Wave Imaging Using VSP data: Looking up from an Extended-reach Horizontal Well, Extended Abstracts, 71st Mtg.: Eur. Assn. Geosci. Eng., Amsterdam, 2009.

Haldorsen, J.B.U., M. Milenkovic, N.J. Brooks, C. Crowell, and M.B. Farmani, 2012a. A Full-waveform, Migration-based Deconvolution Approach to Locating Micro-seismic Events, Paper D020, Extended Abstracts, 74th Mtg.: Eur. Assn. Geosci. Eng., Copenhagen, 2012.

Haldorsen, J.B.U., M. Milenkovic, N. Brooks, C. Crowell, and M.B. Farmani, 2012b. Locating Microseismic Events using Migration-based Deconvolution, Expanded Abstracts SEG Meeting.

Haldorsen, J. B. U., Miller, D. E. and Walsh, J. J. 1994. Multichannel Wiener deconvolution of vertical seismic profiles. Geophysics, **59**, 1500-1511.

Leaney, W. S, and C. Esmersoy, 1989, Parametric Decomposition of Ofseet VSP wave fields: Expanded Abstracts SEG Meeting.

Miller, D., Oristaglio, M. and Beylkin, G. 1987. A new slant on seismic imaging: Migration and integral geometry. Geophysics, **52**, 943-964.

Schuster, G. T., 2002, Reverse-Time Migration = Generalized Diffraction Stack Migration: Expanded Abstracts SEG Meeting.

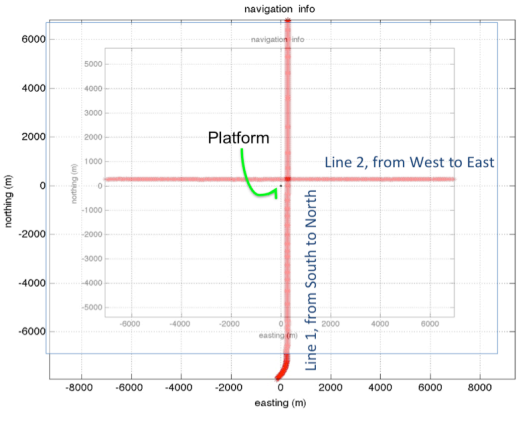

Figure 1. The geometry of two 15-20 km long walk-away VSP lines, intersecting near a platform. The 40 3C receivers are deployed in a near-vertical well below the platform.

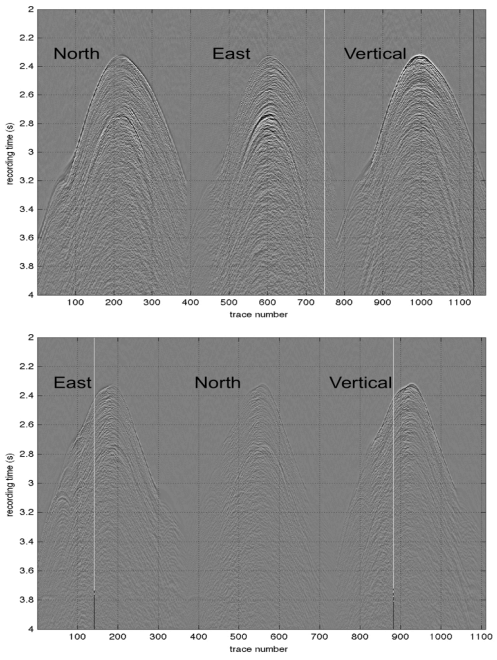

Figure 2. Raw, oriented data recorded at the shallowest receiver level from the two walk-away lines: South-North on top, and West-East on the bottom.

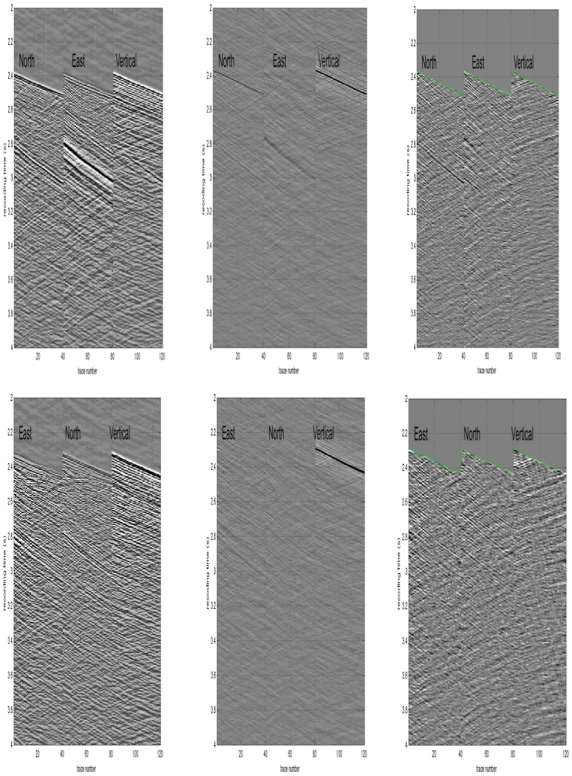

Figure 3. Common shot-point gathers for a shot near the platform: South-North on top, and West-East on bottom; raw data on the left, deconvolved data in the middle, and residuals after separating the down-going P from the deconvolved data. For each line, the data components are sorted in the order: in-line, transverse, and vertical.

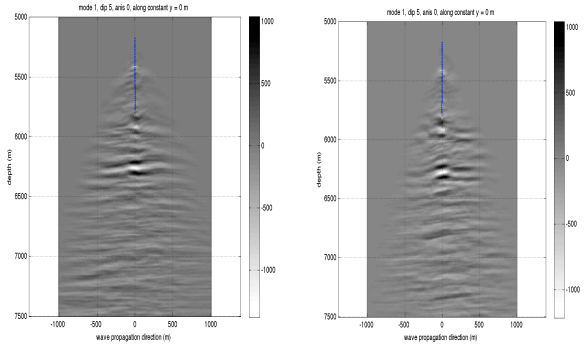

Figure 4. Migrated images derived from the residuals after removing estimates of the down-going P from the deconvolved data: the source line from South to North on left, and the source line from the West to East on right.

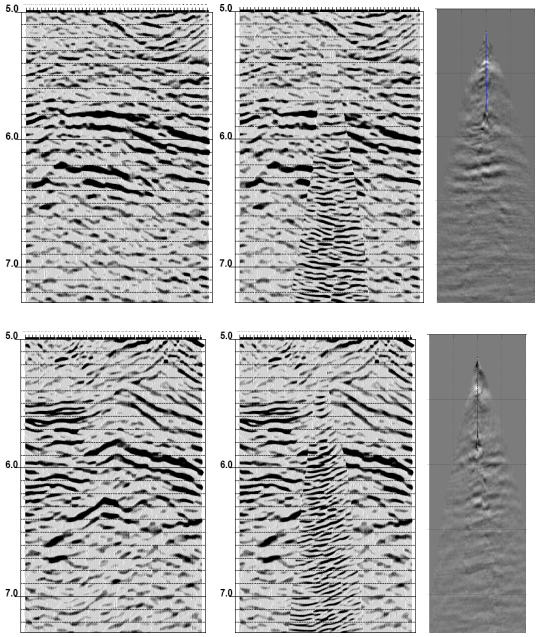

Figure 5. Images obtained from surface-seismic data (on the left) and these images with the images obtained by conventional processing of the walk-away line (in the middle). On the right are the images obtained from vector migration, compensated for varying fold (or energy flux density) as calculated for each image pixel.